Наносистеми, наноматеріали, нанотехнології
Nanosistemi, Nanomateriali, Nanotehnologii
2019, т. 17, № 2, сс. 299–310

PACS numbers: 68.37.Hk, 72.80.Tm, 77.84.Lf, 81.05.U-, 81.16.-c, 82.45.Yz, 82.47.Uv

Synthesis, Structural, Morphological, Electrical, and Electrochemical Properties of $Ni(OH)_2$/Reduced Graphene Oxide Composite Materials

V. M. Boichuk, Kh. V. Bandura, V. O. Kotsyubynsky, I. P. Yaremiy, and S. V. Fedorchenko

Vasyl Stefanyk Precarpathian National University,
57, Shevchenko Str.,
UA-76000 Ivano-Frankivsk, Ukraine

The paper presents the experimental results of the composite-materials' synthesis on the base of nickel hydroxide β-$Ni(OH)_2$ and reduced graphene oxide using ultrasound dispersion of hydrothermally obtained β-$Ni(OH)_2$ and previously chemically reduced graphene oxide. The synthesized material is investigated by XRD, SEM, and impedance spectroscopy. The increasing of composite dispersion degree at increasing of carbon-component content is observed. The electrical conductivity of pure β-$Ni(OH)_2$ and *r*GO, and β-$Ni(OH)_2$/*r*GO composite materials at different ratios of components is analysed at different frequencies in the temperature range of 25–200°C. The decrease in the activation energy of an electric conductivity for the β-$Ni(OH)_2$/*r*GO nanocomposite at the component ratio of 1:2, in comparison with pure *r*GO, is observed.

У роботі представлено експериментальні результати синтези композитних матеріялів на основі гідроксиду ніклю β-$Ni(OH)_2$ і відновленого оксиду графену методою ультразвукового дисперґування гідротермально одержаного β-$Ni(OH)_2$ і попередньо хемічно відновленого оксиду графену (*r*GO). Синтезований матеріял досліджували за допомогою аналізи дифракції Х-променів, сканувальної електронної мікроскопії та імпедансної спектроскопії. При збільшенні вмісту вуглецевого компоненту спостерігалося збільшення ступеня дисперсности композиту. Проведено аналізу електропровідности чистих β-$Ni(OH)_2$ і *r*GO, а також композитних матеріялів β-$Ni(OH)_2$/*r*GO при різному співвідношенні компонентів при різних частотах в інтервалі температур 25–200°C. Спостерігалося зменшення енергії активації електричної провідности для нанокомпозиту β-$Ni(OH)_2$/*r*GO при співвідношенні компонентів 1:2, порівняно з чистим *r*GO.

В работе представлены экспериментальные результаты синтеза компо-

зитных материалов на основе гидроксида никеля β-$Ni(OH)_2$ и восстановленного оксида графена методом ультразвукового диспергирования гидротермально полученного β-$Ni(OH)_2$ и предварительно химически восстановленного оксида графена (*r*GO). Синтезированный материал исследовали с помощью анализа дифракции рентгеновских лучей, сканирующей электронной микроскопии и импедансной спектроскопии. При увеличении содержания углеродного компонента наблюдалось увеличение степени дисперсности композита. Проведён анализ электрической проводимости чистых β-$Ni(OH)_2$ и *r*GO, а также композитных материалов β-$Ni(OH)_2$/*r*GO при различном соотношении компонентов при различных частотах в интервале температур 25–200°C. Наблюдалось уменьшение энергии активации электрической проводимости для нанокомпозита β-$Ni(OH)_2$/*r*GO при соотношении компонентов 1:2, по сравнению с чистым *r*GO.

Key words: nickel hydroxide, reduced graphene oxide, ultrasound dispersion, hydrothermal synthesis, electrical conductivity, electrochemical properties.

Ключові слова: гідроксид ніклю, відновлений оксид графену, ультразвукове дисперґування, гідротермальна синтеза, електропровідність, електрохемічні властивості.

Ключевые слова: гидроксид никеля, восстановленный оксид графена, ультразвуковое диспергирование, гидротермальный синтез, электрическая проводимость, электрохимические свойства.

(Received 15 April 2019; in final form, 22 April 2019)

1. INTRODUCTION

Electrochemical capacitors (EC) due to its power, long cyclic capability and low cost are the excellent solution for novel energy-storage systems for back-up energy devices of renewable sun and wind sources or electric vehicles. There are two different charge storage mechanisms for EC. The first one is based on the electrostatic electric double layer (EDL) formation at the electrode/electrolyte interface during electroadsorption of solvated ions from liquid electrolyte [1]. Another one includes the reversible or semi-reversible Faradaic redox reactions with the dependence of accumulation charge on the electrode potential, which causes electrochemical pseudo-capacitance [2]. The large specific capacitance value of EDL devices (up to hundreds of farads per gram) is a result of very short distance between charged layers separated by electrode/electrolyte interface and very high specific surface area value of electrode materials (up to 3000 $m^2 \cdot g^{-1}$) typically based on the porous carbon materials. The redox mechanisms allow accumulating

relatively higher specific capacitance and energy density values compared to the ones for EDL. The main requirement for pseudo-capacitive electrode is the realization of surface and bulk redox process in combination with intercalation of electrically active species (ions from electrolyte) into channels and interlayer space of crystal lattice of electrode materials. The reversible redox activity, high specific surface area and high electrical conductivity are crucially important and simultaneously mutually contradictory demands for high performance for pseudo-capacitors electrode. The EDL capacitors have an extremely high power density value and cycling ability, but specific energy densities are relatively low (up to 12 $Wh \cdot kg^{-1}$ for the best commercial devices) [3]. At the same time, pseudo-capacitors demonstrate too low power density and low lack of cycling stability for commercial use. The development of hybrid systems that combine Faradaic electrode (energy source) and EDL electrode (power source) allows obtaining a high performance electrochemical cell [4, 5]. The main problem is maintaining the redox reactions reversibility that depends on the battery-type electrode properties and a correct functionality of all components of EC as a unified system. The development of a novel electrode material is crucially important for next technological progress in this branch. Among the perspective materials for Faradaic electrode (RuO_2, MnO_2, MoO_3), nickel hydroxide β-$Ni(OH)_2$ has a high theoretical specific capacitance (of about 2358 $F \cdot g^{-1}$ [6]), but very low electrical conductivity restricts its using. The formation of β-$Ni(OH)_2$–reduced graphene oxide (*r*GO) composite materials allows improving the electrochemical properties of this material.

2. EXPERIMENTAL DETAILS

Ultrafine β-$Ni(OH)_2$ was synthesized by hydrothermal route. The sol obtained by the interaction of $NiCl_2 \cdot 6H_2O$ and ammonia solutions with the presence of PEG 6000 as a surfactant was placed in teflon-lined autoclave and then was kept at the temperature of 120°C for 8 h. The obtained green precipitate was washed until pH = 7 and dried at 60°C. Graphene oxide (GO) was synthesized by modified Hummers method using protocol described in [7]. Graphite fine powder (5 g) and sodium nitrate (2.5 g) were mixed with concentrated sulphur acid (110 ml, 98%) in the ice bath at the temperature of about 0°C. Potassium permanganate (15 g) was slowly added to the mixture at the temperature of about 15–20°C. The purification of GO from Mn ions was realized by addition of sodium hydroxide up to pH = 10 with the removing of the formed precipitate. The obtained colloidal mixture was heated up to 35°C and stirring for 3 hours. Deionized water (230 ml) was added dropwise to the obtained reaction medium with next

its heating up to 95°C and continuous stirring for 1 hour. The deionized water (360 ml) and Hydrogen peroxide (40 ml, 30%) were added to the mixture. After cooling to room temperature, the obtained colloidal suspension was ultrasonicated for 4 hours and centrifuged to provide removing of unexfoliated graphite particles, filtered, washed by HCl and distilled water/ethanol mixture for sulphate species removing. The final dark yellow precipitate was dried in vacuum at 60°C. GO reduction was carried out under the hydrothermal conditions with the presence of hydrazine hydrate. β-$Ni(OH)_2$/*r*GO composite was obtained by ultrasound dispersion of β-$Ni(OH)_2$ and *r*GO (mass ratio of 2:1, 1:1 and 1:2, respectively) in distilled water.

The phase composition and structure of the synthesized materials were analysed by XRD and SAXS on a DRON-3M powder diffractometer (CuK_α radiation). The average size of coherent scattering domains (CSD) was calculated by Scherrer's formula.

The frequency dependence of electrical conductivity was investigated by impedance spectroscopy (Autolab PGSTAT 12/FRA-2 device) in the frequency range of 0.01–100 kHz at temperatures of 20–200°C. The electrical conductivity value was measured for cylindrical samples prepared by pressing at 20 kN.

Vega 3 MLN TESCAN device Scanning Electron Microscope was used for testing of morphological characteristics of the samples.

Ultrasonic treatment was performed using disperser 'USDN-A' (working frequency of 20–25 kHz).

Electrochemical measurements were realized with a three-electrode cells consisted of working electrode (electrode composition on the pure Ni substrate) reference electrode (Ag/AgCl), counter electrode (platinum wire). Electrode composition consists of 90% active material, 5% acetylene black and 5% polyvinylidene fluoride mixed with acetone and dried at 80°C for 3 hours. 6M·KOH aqueous solution was used as an electrolyte. Cyclic voltammetry measurements were done at scan rate of 1, 2, 3, 4, 5, 10 $mV \cdot s^{-1}$.

3. RESULTS AND DISCUSSION

The XRD patterns of the pure *r*GO, β-$Ni(OH)_2$, and β-$Ni(OH)_2$/*r*GO composite are shown in Fig. 1. All patterns were processed with the PowderCell software [8]. According to XRD data, all the synthesized samples form hexagonal β-$Ni(OH)_2$ phase (JCPDS 38-0715) with HO–Ni–OH layers that are arranged along crystallographic direction **c** with octahedral coordination of Ni^{2+} ions.

The broadening of (001) diffraction peak is an evidence of dominant particle growth (average size of about 15 nm) along the [100] and [110] directions that causes plate-like morphology. This conclusion is confirmed by direct observation using SEM method (Fig. 2).

The preferred orientation degree of β-$Ni(OH)_2$ crystallites was calculated by analysis of intensity ratio between (001) and (101) reflexes for composite materials with different *r*GO contents. The increasing of intensity ratio between (001) and (101) with the increasing of *r*GO content was observed. It corresponds to increasing of the preferred growth degree. It can be assumed that ultrasonic dispersion causes the decreasing of average particles sizes of materials

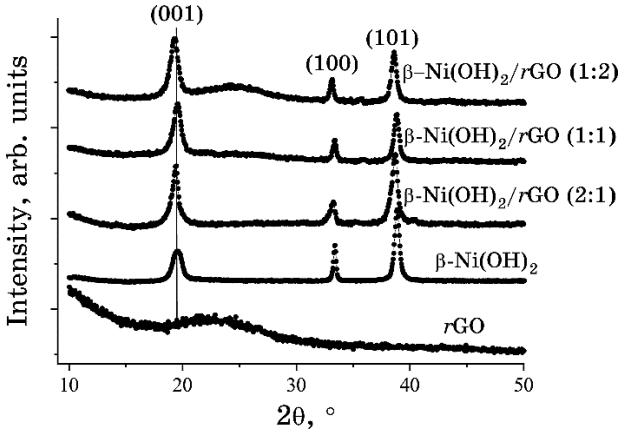

Fig. 1. XRD patterns of β-$Ni(OH)_2$, *r*GO and β-$Ni(OH)_2$/*r*GO composite materials at different ratio components.

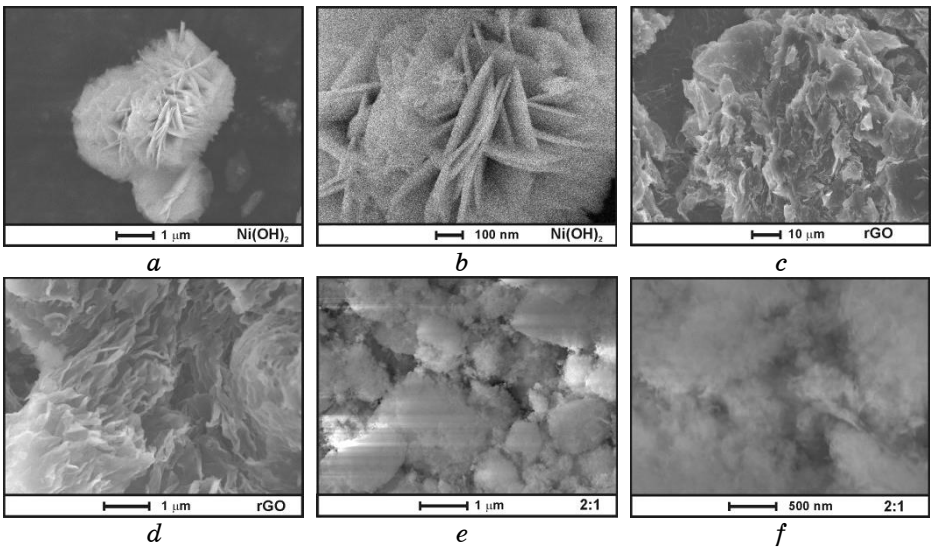

Fig. 2. SEM images of β-$Ni(OH)_2$ (*a*, *b*), *r*GO (*c*, *d*) and β-$Ni(OH)_2$/*r*GO (*e*, *f*, *g*, *h*, *i*, *j*) composite materials at different components ratio.

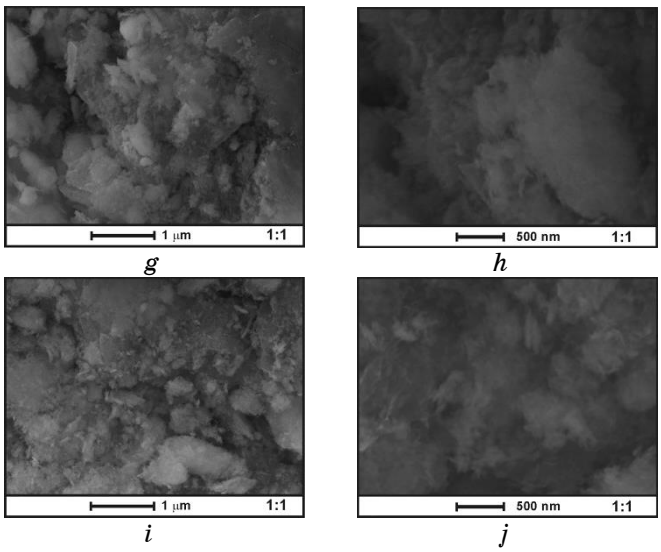

g *h* *i* *j*

Continuation of Fig. 2.

with possibility of carbon atoms insertion into the interplanar space of β-$Ni(OH)_2$ that is in a good agreement with SEM data (Fig. 2).

The electrical conductivity mechanisms for pure β-$Ni(OH)_2$ and *r*GO, and β-$Ni(OH)_2$/*r*GO composite materials at different components ratio were analysed by impedance spectroscopy at temperatures of 25–200°C (Fig. 3). The non-linear temperature dependences of the β-$Ni(OH)_2$ electric conductivities at some selected frequencies demonstrate the presence of maximum at 125°C with next decreasing of conductivity. The observed phenomena are caused by the dominance of protonic conductivity in β-$Ni(OH)_2$ with the hopping mechanism of charge carriers [9]. The temperature increasing leads to water molecules removing from interplanar space and it changes the electrical conductivity mechanism. The slight changes in the conductivity at low frequencies and its increase with frequency increasing were observed for the sample at measurement temperatures of 175 and 200°C that is typical for disordered semiconductors. Jonscher power law was used to interpret the relaxation frequency of electrical conductivity: $\sigma(\omega) = \sigma_{dc} + A\omega^n$, where σ_{dc} is the *dc* conductivity, *A*—prefactor, and *n* is a frequency exponent parameter ($0 < n < 1$) characterizing the deviation from Debye behaviour and measurement of the interionic coupling strength [10]). Calculated values of *n* are 0.41±0.06 and 0.95 ± 0.05 for curves obtained at 175 and 200°C, respectively. The range of $0 < n < 0.4$ is an evidence of charge transferring through the system of conductive grains separated by less conductive barriers, which behave as macroscopic di-

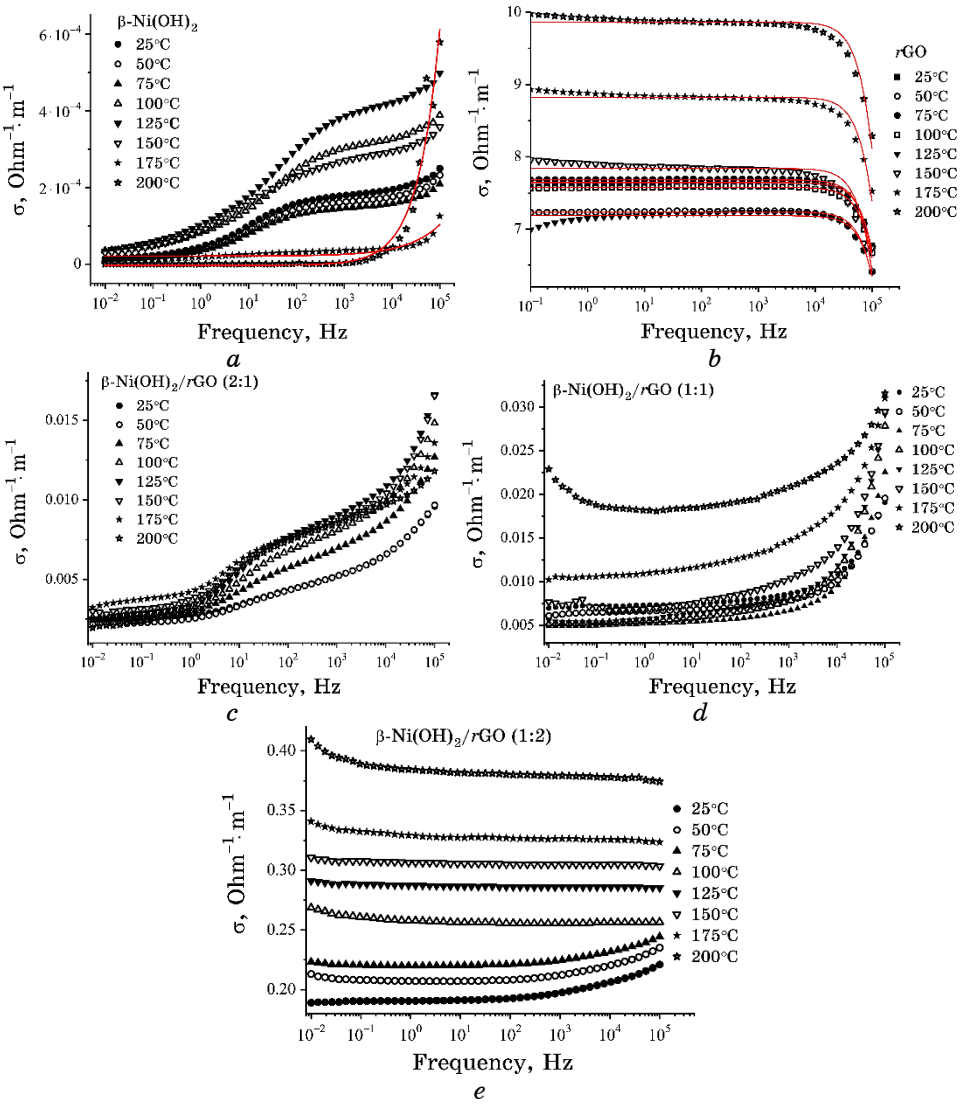

Fig. 3. The frequency dependence of electrical conductivity of β-$Ni(OH)_2$ (*a*), *r*GO (*b*) and β-$Ni(OH)_2$/*r*GO (*c*, *d*, *e*) composite materials at different temperatures (solid lines are fitting results of Eq. (1)).

poles strongly interacting with each other [11].

The exponent range of $0.4 < n < 0.6$ suggests multipolaron hopping of charge carriers across the grains interfaces boundaries [12]. The obtained result indicates the transition from diffusively limited character of carrier hops between quasi-equilibrium positions in the crystal lattice separated by a potential barrier and correlated barri-

er-hopping mechanism of conductivity.

The decreasing of specific electrical conductivity that is observed for pure *r*GO at frequencies >1000 Hz corresponds to electric current distribution near the surface of conducting graphene packages (skin effect) [13]. In this case, $\sigma(\omega, T)$ curves can be fitted by Drude model as $\sigma(T) = \frac{\sigma_{dc}}{1 + \omega^2 \tau^2(T)}$, where σ_{dc} is a direct current conductivity.

The slight change in $\sigma_{dc}(T)$ in a range of 25–100°C with the next linear growth was observed. Both σ_{dc} depend on the temperature following Arrhenius law: $\sigma_{dc}(T) = \sigma_0 \exp\left[-\frac{E_a}{kT}\right]$, where E_a is activation energy, σ_0 and τ_0 are prefactors [14]. The calculated value of activation energy is 0.07 eV.

The increasing of *r*GO component relative content in composite materials leads to a systematic evolution of the electric conductivity spectra. The characteristic changes are also observed at the increasing of experiment temperature. The effect of *r*GO component for β-$Ni(OH)_2$/*r*GO (2:1) composite material corresponds to additional conductivities increasing in the frequency range of about 10^0–10^2 Hz (Fig. 3). Highly sensitive behaviour of temperature dependences of electrical conductivity on the frequency was observed for this sample. This effect is a result of two components presence with different conduction mechanisms that are dominant at different temperatures and frequency ranges (Fig. 4, *a*). It can be assumed that the increase in temperature or signal frequency causes the enlarg-

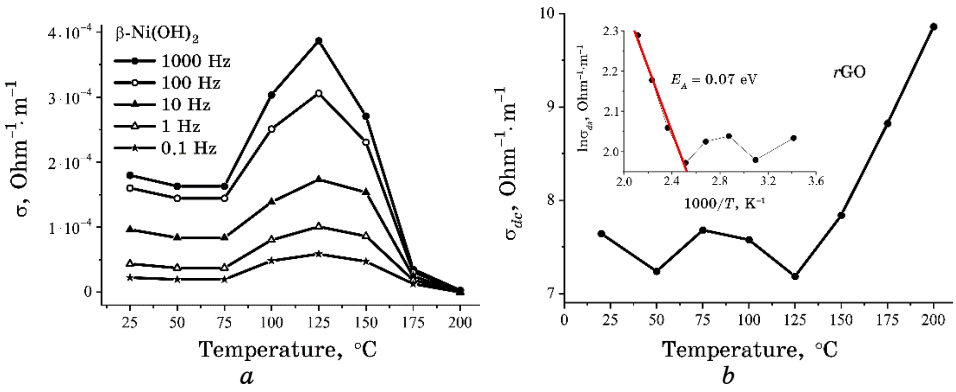

Fig. 4. The temperature dependences of specific electrical conductivities for pure β-$Ni(OH)_2$ at selected frequencies (*a*) and σ_{dc} parameter for *r*GO sample at different temperatures with corresponding Arrhenius plot (*b*).

ing of carbon component influence. This assumption is confirmed by the temperature dependences of electrical conductivity of β-$Ni(OH)_2$/*r*GO (1:1). The slow increase in electrical conductivity in the low-frequency region with its gradual increasing and a jump in the high-frequency region are observed for all the temperatures less than 200°C (Fig. 3). The gradual increase in the low-frequency electrical conductivity was observed for this temperature. The same effect for composite material with highest *r*GO content (β-$Ni(OH)_2$/*r*GO (1:2)) was observed at temperatures more than 100°C. Temperature dependences of electrical conductivity for this material became frequency-independent that allow calculating an activation energy value (Fig. 5, *d*). The calculated value of activation energy is about 0.06 eV that corresponds to better electrical conductivity of composite system.

Cyclic voltammetry method was used for testing of electrochemical performance of all the synthesized materials in 6M·KOH aqueous solution (Fig. 6).

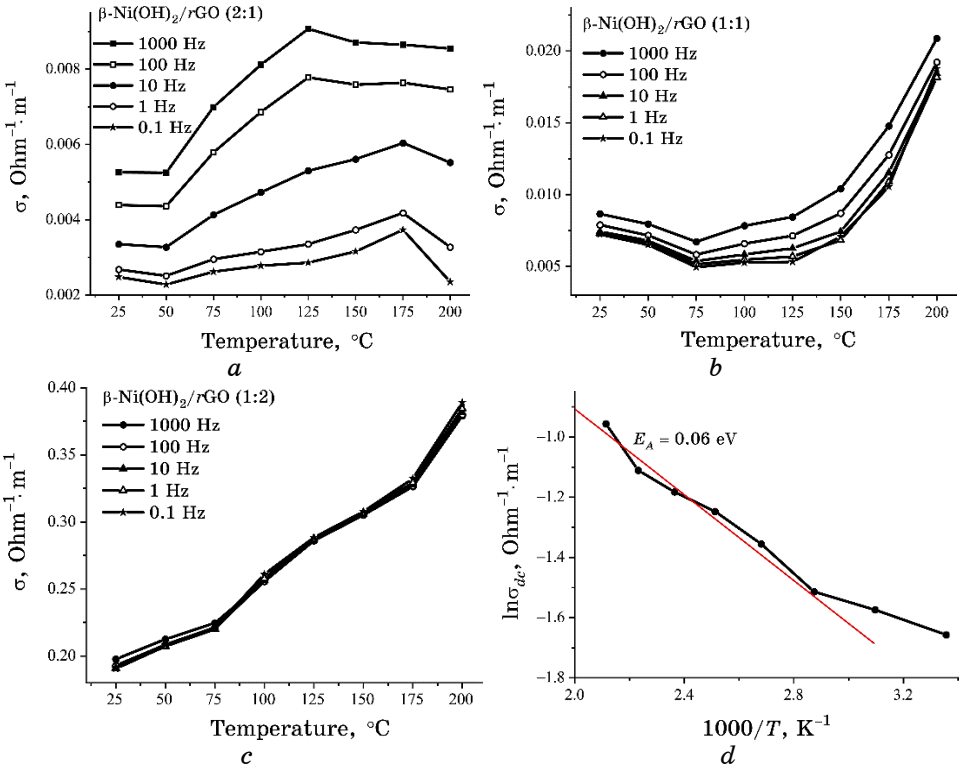

Fig. 5. Temperature dependences of electrical conductivity for β-$Ni(OH)_2$–*r*GO composites at different frequencies.

As can be seen from Fig. 6, *a*, all the CVA curves measured for *r*GO electrodes exhibit almost close to rectangular shapes in the range of 0 V to 0.5 V that is the evidence of a reversible capacitive

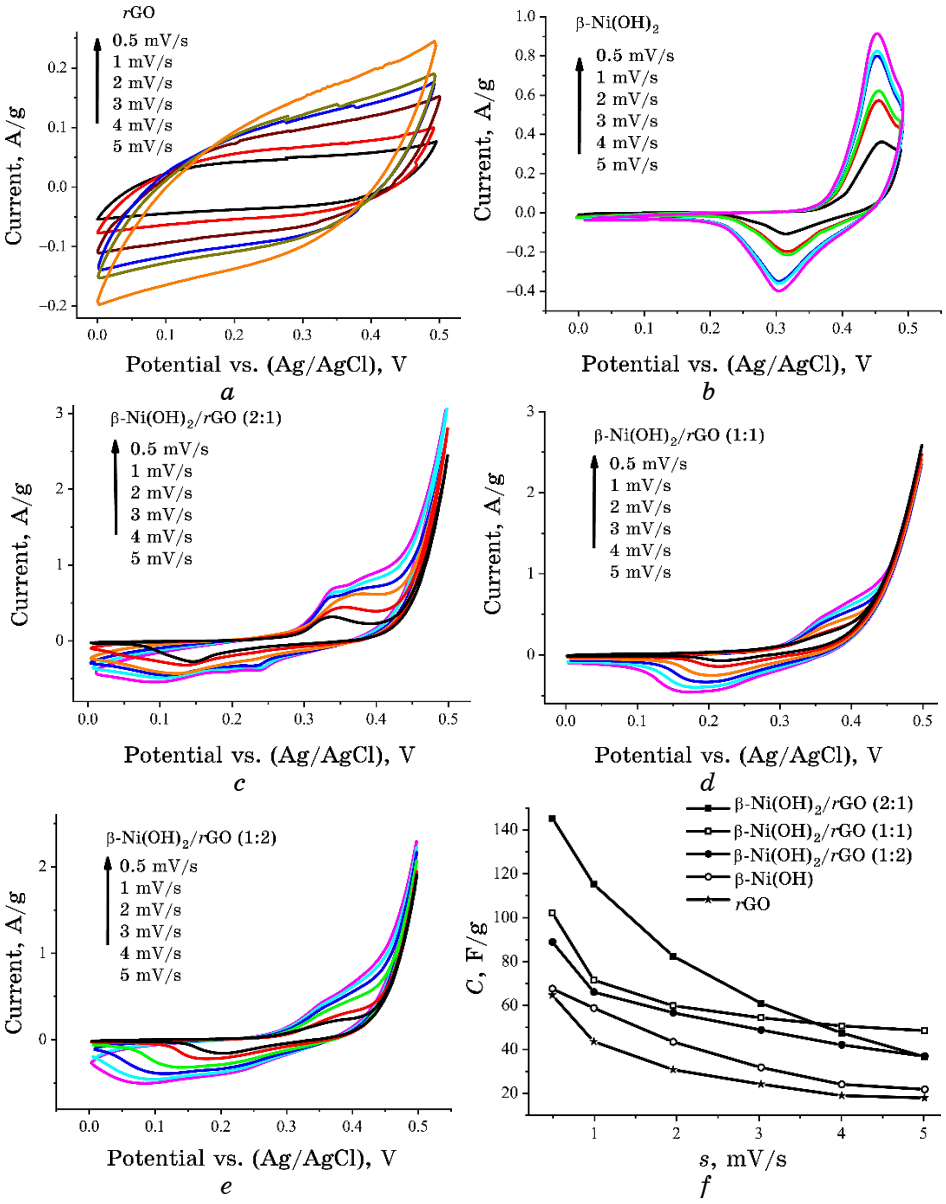

Fig. 6. Cyclic voltammograms obtained at various scan rate for electrode based on (*a*) *r*GO, (*b*) β-$Ni(OH)_2$ and (*c*, *d*, *e*) β-$Ni(OH)_2$/*r*GO (*c*) composites, and (*f*) the dependences of capacitance on scan rate.

behaviour of charge accumulation. The transformation of CVA curves with scan rate increasing is typical for EDL charge accumulation type [15]. The pair of well-defined redox peaks is observed on CVA plots of $Ni(OH)_2$-based electrode (Fig. 6, *b*) that corresponds to the Faradaic reactions [16] $\beta\text{-}Ni(OH)_2 + OH^- \leftrightarrow NiOOH + H_2O + e^-$. The symmetry of anodic and cathodic peaks is a result of the reversible process behaviour and measured charge storage are caused by pseudocapacitive mechanism. The redox processes are observed on the CVA response measured for composite electrodes (Fig. 6, *c*–*e*) but in this case the peaks are broadened and changes in shape of CVA curves with the scan rate increasing are not significant. This indicates both complex character of electrode capacitance and better charge carriers transport through the electrode material.

The values of average specific capacitances (C) were calculated using the area under the CVA curves as a function of potential scan rate [16]: $C = \int_{U_1}^{U_2} I(U)dU \Big/ 2ms(U_2 - U_1)$, where U_1 and U_2 are cut-off potentials, $I(U)$ is a current, m is a mass of active electrode material, s is a scan rate. The values of specific capacitance for *r*GO- and $\beta\text{-}Ni(OH)_2$-based electrodes change from 65 to 18 $F \cdot g^{-1}$ and from 68 to 22 $F \cdot g^{-1}$ with the scan rate increasing in a range of 0.5–5 $mV \cdot s^{-1}$ (Fig. 6, *f*). $\beta\text{-}Ni(OH)_2$/*r*GO composite with maximal $\beta\text{-}Ni(OH)_2$ content demonstrates the best capacitive response (145 $F \cdot g^{-1}$ at $s = 0.5$ $mV \cdot s^{-1}$) with the maximal decrease in specific capacitances with the scan rate increasing. The increasing of carbon component content leads to the deterioration of capacitive properties. The maximal specific capacitance values for the $\beta\text{-}Ni(OH)_2$/*r*GO composites are 102 and 89 $F \cdot g^{-1}$ at component ratio 1:1 and 1:2, respectively.

4. CONCLUSIONS

Simple and effective hydrothermal synthesis of $\beta\text{-}Ni(OH)_2$/*r*GO using ultrasonic dispersion of hydrothermally synthesized $\beta\text{-}Ni(OH)_2$ and chemically reduced graphene oxide is proposed. The preferred orientation of $\beta\text{-}Ni(OH)_2$ crystallites in (001) crystallographic plane was observed. The increasing of carbon component in composite material leads to the increase in sample dispersion degree. The increasing of interplanar distance along crystallographic direction **c** for $\beta\text{-}Ni(OH)_2$/*r*GO composite (components' ratio of 1:2) can be explained by insertion of carbon atoms. The frequency dependencies of conductivity of initial components ($\beta\text{-}Ni(OH)_2$ and *r*GO) and composite materials at different components' ratio were investigated. The protonic conductivity mechanism is dominating for pure $\beta\text{-}Ni(OH)_2$ up to 150°C. Activation energy of electronic conductivity for reduced

graphene oxide was about 0.07 eV. The frequency and temperature dependences of electrical conductivities were observed for the samples with component ratio of 1:2 and 1:1. The formation of β-$Ni(OH)_2$/*r*GO nanocomposite at component ratio of 1:2 leads to frequency-independent conductivity with activation energy value of about 0.06 eV. The dominating of electrostatic and Faradaic capacitance response was observed for *r*GO- and β-$Ni(OH)_2$-based electrodes, respectively. The maximal capacitive performance was observed for β-$Ni(OH)_2$/*r*GO composite with component ratio of 2:1. The specific capacitance increasing for β-$Ni(OH)_2$/*r*GO system in comparison with pure components is a result of increase in both electron and ion transfer due to the increase in conductivity and electrode/electrolyte interface area.

REFERENCES

1. L. L. Zhang and X. S. Zhao, *Chem. Soc. Rev.*, **38**, No. 9: 2520 (2009).
2. E. Frackowiak, *Phys. Chem. Chem. Phys.*, **9**, No. 15: 1774 (2007).
3. H. Ji, X. Zhao, Z. Qiao, J. Jung, Y. Zhu, Y. Lu, and R. S. Ruoff, *Nat. Commun.*, **5**: 3317 (2014).
4. A. González, E. Goikolea, J. A. Barrena, and R. Mysyk, *Renewable Sustainable Energy Rev.*, **58**: 1189 (2016).
5. L. O. Shyyko, V. O. Kotsyubynsky, I. M. Budzulyak, and P. Sagan, *Nanoscale Res. Lett.*, **11**, No. 1: 243 (2016).
6. L. Soserov, T. Boyadzhieva, V. Koleva, A. Stoyanova, and R. Stoyanova, *ECS Trans.*, **74**, No. 1: 213 (2016).
7. D. C. Marcano, D. V. Kosynkin, J. M. Berlin, A. Sinitskii, Z. Sun, A. Slesarev, and J. M. Tour, *ACS Nano*, **4**, No. 8: 4806 (2010).
8. W. Kraus and G. Nolze, *J. Appl. Crystallogr.*, **29**, No. 3: 301 (1996).
9. S. Deabate, F. Henn, S. Devautour, and J. C. Giuntini, *J. Electrochem. Soc.*, **150**, No. 6: J23 (2003).
10. J. C. Dyre and T. B. Schroder, *Rev. Mod. Phys.*, **72**, No. 3: 873 (2000).
11. A. Jonscher, *J. Non-Cryst. Solids*, **8**, No. 10: 293 (1972).
12. N. Naresh and R. Bhrowmik, *J. Phys. Chem. Solids*, **73**, No. 2: 330 (2012).
13. F. Wu, A. Xie, M. Sun, Y. Wang, and M. Wang, *J. Mater. Chem. A*, **3**, No. 27: 14358 (2015).
14. K. Chakraborty, S. Chakrabarty, T. Pal, and S.Ghosh, *New J. Chem.*, **41** No. 11: 4662 (2017).
15. J. Lazarte, R. Dipasupil, G. Pasco, R. Eusebio, A. Orbecido, R. A. Doong, and L. Bautista-Patacsil, *Nanomater.*, **8**, No. 11: 934 (2018).
16. M. Aghazadeh, A. N. Golikand, and M. Ghaemi, *Int. J. Hydrogen Energy*, **36**, No. 14: 8674 (2011).